This is the Pre-Published Version.

This document is the Accepted Manuscript version of a Published Work that appeared in final form in Chemistry of materials, copyright © 2017 American Chemical Society after peer review and technical editing by the publisher. To access the final edited and published work see https://doi.org/10.1021/acs.chemmater.7b02346.

Dopant Induced Impurity Bands and Carrier Concentration Control for Thermoelectric Enhancement in p-Type $Cr_2Ge_2Te_6$

Xiaodan Tang[a,c,‖], Dengdong Fan[b,‖], Kunling Peng[a,c], Dingfeng Yang[e], Lijie Guo[a], Xu Lu[a], Jiyan Dai[d], Guoyu Wang[c], Huijun Liu[b,*], Xiaoyuan Zhou[a,*]

[a]College of Physics, Chongqing University, Chongqing 401331, P. R. China.

[b]Key Laboratory of Artificial Micro- and Nano-Structures of Ministry of Education and School of Physics and Technology, Wuhan University, Wuhan 430072, P. R. China.

[c]Chongqing Institute of Green and Intelligent Technology, Chinese Academy of Sciences, Chongqing, 400714, P. R. China.

[d]Department of Applied Physics, The Hong Kong Polytechnic University Kowloon, Hong Kong.

[e]Institute of Microstructure and Properties of Advanced Materials, Beijing University of Technology, Beijing, 100124, P. R. China.

[‖] Authors have contributed equally to this work.

Supporting Information

ABSTRACT: Our previous work demonstrated that $Cr_2Ge_2Te_6$ based compounds with a layered structure and high symmetry are good candidates for thermoelectric application. However, the power factor of only ~0.23 mW/mK^2 in undoped material is much lower than that of conventional thermoelectrics. This indicates the importance of an electronic performance optimization for further improvements. In this work, either Mn- or Fe-substitution on Cr site are investigated, with expectations of both carrier concentration control and band structure engineering. First-principle calculations indicate that an orbital hybridization between *d* orbitals of the doping atom and the *p* orbital of Te significantly increase the density of states (DOS) around Fermi level. In addition, it is found that Mn-doping is more favorable to improve the electrical properties than Fe doping. By tuning the carrier concentration via Mn doping, the peak power factor rises rapidly from 0.23 mW/mK^2 to 0.57 mW/mK^2 at 830 K with x = 0.05. Combined with the intrinsic low thermal conductivity, $Cr_{1.9}Mn_{0.1}Ge_2Te_6$ displays a decent *zT* of 0.63 at 833 K, a twofold value as compared to that of undoped sample at same direction and temperature.

INTRODUCTION

Thermoelectric (TE) materials can directly convert temperature gradients into available electricity, attracting greatly increasing attention for promising application in waste heat recovery.[1] A high conversion efficiency of heat to electricity is desirable and needed for practical application. According to TE efficiency formula

$$\eta = \frac{T_H - T_C}{T_H}\frac{\sqrt{1+ZT}-1}{\sqrt{1+ZT}+\frac{T_C}{T_H}}$$

where T_H and T_C are the hot-end and cold-end temperatures of the thermoelectric materials, respectively, top-notch thermoelectric materials should possess a high dimensionless thermoelectric figure of merit *zT*, defined as $zT = S^2\sigma T/\kappa$, where S, σ, T, κ are the Seebeck coefficient, the electrical conductivity, the absolute temperature, the thermal conductivity, respectively.[2-5] The problem is that the transport parameters are interdependent and, often, attempts to maximize one parameter have a deleterious effect on the other parameters.[6] There are two general strategies to improve the *zT* of a thermoelectric material: increasing numerator power factor ($S^2\sigma$), or reducing the total thermal conductivity. With regards to the first strategy, many approaches such as introducing band convergence,[7,8] and nestification,[9] electron energy barrier filtering,[10,11] quantum confinement effects[12] and using the resonant level[13] have been proved successful. Equally impressive gains have been achieved using the time-honored strategy of reducing the thermal conductivity, i.e., isolated Einstein-like modes (rattlers) in the oversized structural voids,[14,15] strategically placed point defects,[16,17] all-scale hierarchical structure,[18] low sound velocity[19] and multiple scattering mechanisms.[20] As a consequence, exceptionally high peak value of *zT* exceed to 2.0 has been obtained.[21,22]

Recently, the $Cr_2Ge_2Te_6$ compounds, a substantially two-dimensional semiconductor, have been reported as a promising thermoelectric materials.[23] In this compound, Tellurium anions form a hexagonally closed packed structure along the c-axis. 2/3 of the octahedral cavities are occupied by chromium within every other layer, leaving behind a completely open gap along the c-axis. The intra-layer arrangement of the $CrTe_6$ octahedral is honeycomb-like, with a dimer of germanium inserted perpendicularly in each center position of the $CrTe_6$ two dimensional net resulting in interesting ethane-like species [Ge_2Te_6]. It should be mentioned that there exist various chemical bonds in $Cr_2Ge_2Te_6$, including Cr-Te ionic bonds, Ge-Te covalent bonds, Ge-Ge metal bonds, and the inter-layer van der Waals bonds. Such mix-bonded systems are believed to generate partially localized low frequency phonon modes, low sound velocities, and large phonon anharmonicities, which are all favorable for achieving a low lattice thermal conductivity.[24-27]

In our previous study,[23] it is found that the compacted undoped $Cr_2Ge_2Te_6$ sample displays a moderate *zT* value of 0.38 and 0.33 along the direction that are perpendicular (P) to the pressing direction and parallel to the pressing directions (A) at 833 K, respectively. The thermal conductivity is further reduced by introducing Cr defects ($Cr_{1.94}Ge_2Te_6$) and the $(zT)_{max}$ then reaches 0.45 along A direction. This work is a very successful initial study which proves that $Cr_2Ge_2Te_6$ with a layered structure is good candidate for thermoelectric application. However, it is noted that the carrier concentration in pure $Cr_2Ge_2Te_6$ sample is around 5E17

cm^{-3}. With the introduction of Cr defects, the carrier concentration was not raised. As a consequence, the power factor was not improved as expected via introducing Cr deficiency. Actually, According to the spin polarized band structure[28] of $Cr_2Ge_2Te_6$, the material is an indirect and multi-band semiconductor. One notes doubly degenerate valence bands at the Γ point which, together with the trigonal symmetry of the crystal structure, assure the existence of multiple carrier pockets. Given the fact that an additional valence band at the Γ point is merely 0.1 eV below, it may contribute to transport when the structure is doped or when the temperature is raised. Thus, there is a good chance that the Seebeck coefficient would benefit from the presence of all three differently dispersive valence bands and the structure would also support high electrical conductivity. Thus, based on our assessment, it seems plausible to achieve high power factors in $Cr_2Ge_2Te_6$ by proper chemical modifications to alter the charge carrier concentration and modify the electronic bands. Combined with an intrinsic low and even reduced thermal conductivity by atomic scale alloy scattering, a significant higher thermoelectric performance of $Cr_2Ge_2Te_6$ based compounds can be anticipated.

In this work, we demonstrate the significantly improved thermoelectric performance of $Cr_{2(1-x)}Mn_{2x}Ge_2Te_2$ (x = 0, 0.01, 0.02, 0.03, 0.05) polycrystalline samples from room temperature to 833 K. For comparison, the thermoelectric properties of Fe-doped sample was also investigated. First-principle calculations indicate that an orbital hybridization between *d* orbitals of the doping atom and the *p* orbital of Te introduces additional impurity bands and increases the DOS around Fermi level, significantly increasing the holes concentration upon doping. This greatly improves the electrical conductivity while maintaining a moderate Seebeck coefficient. Besides, the intrinsically layered structure, the mixed-bond characteristics coupled with the pseudo-trigonal symmetry contribute to a low thermal conductivity. Finally, a decent zT~0.63 at 833 K for $Cr_{1.9}Mn_{0.1}Ge_2Te_6$ was obtained along A direction, a twofold value as compared to the undoped sample at same direction and temperature.

EXPERIMENTAL AND THEORETICAL METHODS

Synthesis. $Cr_{2(1-x)}Mn_{2x}Ge_2Te_6$ (x = 0, 0.01, 0.02, 0.03, 0.05) were synthesized by solid-state reaction (SSR) in the sealed quartz tubes and compacted by spark plasma sintering (SPS). High-purity materials (Cr powder, 99.99%; Mn pieces, 99.999%; Fe granule, 99.999%; Ge pieces, 99.999%; Te chunk, 99.99%) in the stoichiometric proportion were weighed about 7 g and then sealed in the vacuum quartz tubes. The loaded tubes were slowly heated to 973 K in 20 h, dwelled at this temperature for 20 h and then naturally drop to room temperature. In order to get pure phase of $Cr_2Ge_2Te_6$ based compounds, the above process was repeated three times. The as-sintered chunks were ground into powders and consolidated into dense bulk samples by SPS at 803 K for 4 minutes under 46 MPa. The final cylindrical products posse density greater than 95% of the theoretical density, and they were subsequently cut into different bulk with appropriate size and shape along A and P directions and subsequently measured electrical and thermal transport properties along both directions.

Measurements. The obtained SPSed samples were cut into rectangular bars with dimensions 8×2.5×2.5 mm for the measurements of Seebeck coefficient (S) and electrical conductivity (σ) on a commercial (Linseis, LSR-3) equipment under the Helium atmosphere. The high density samples were cut into disks with the diameter of 10 mm and the thickness of ~1.4 mm along A direction and 6×6×1.4 mm along P direction for thermal diffusivity λ measurements. The thermal conductivity κ was calculated from $\kappa = \lambda\rho C_P$, where the λ was measured by the laser flash method (Netzsch, LFA 457), ρ (geometric density) was determined by the Archimedes method, and C_p (heat capacity) was estimated using the Dulong Petit approximation (C_p = 25 J/mol*K), respectively. Furthermore, samples were coated with a thin layer of graphite before the thermal diffusivity measurement to minimize errors in the emissivity. The temperature range for measurement of S, σ and κ were from room temperature to 830 K. The estimated errors in the measurements of electrical conductivity, Seebeck coefficient and thermal diffusivity are about 5%, 5% and 3%, respectively. The carrier concentrations of all samples were tested using the van der Pauw technique under a reversible magnetic field of 1.5 T and carrier mobility μ was calculated by the equation $\sigma = nq\mu$. The morphology and microstructure were investigated with field emission scanning electron microscopy (SEM, JSM-7800F, JEOL) and transmission electron microscopy (TEM) studies were carried out using a JEOL 2100F microscope.

Theoretical calculations. The structure optimizations and electronic properties of $Cr_2Ge_2Te_6$ are investigated within the framework of density functional theory (DFT) by using the projector-augmented wave (PAW) method as implemented in the Vienna *ab-initio* simulation package (VASP).[29-31] Since the generalized gradient approximations (GGA)[32] cannot adequately describe the exchange-correlation effects of the strongly localized 3d electrons, we employ the DFT+U method[33] to calculate the electronic properties with spin polarization. The effective Coulomb repulsion parameters U are chosen to be 3.5 eV, 4.0 eV and 4.6 eV for Cr, Mn, and Fe element, respectively.[34] The cut-off energy in the plane wave expansion is set at 600 eV and the energy convergence threshold is 10^{-6} eV. 2×2×2 suppercells with 80 atoms are built for the purpose of randomly replacing Cr atoms with Fe or Mn atoms corresponding to the doping amount of 6.25 percent. For the Brillouin zone integrations, the Monkhorst–Pack scheme with 11×11×11 and 5×5×5 *k*-mesh are respectively employed for the primitive cell and the supercell.

RESULTS AND DISCUSSION

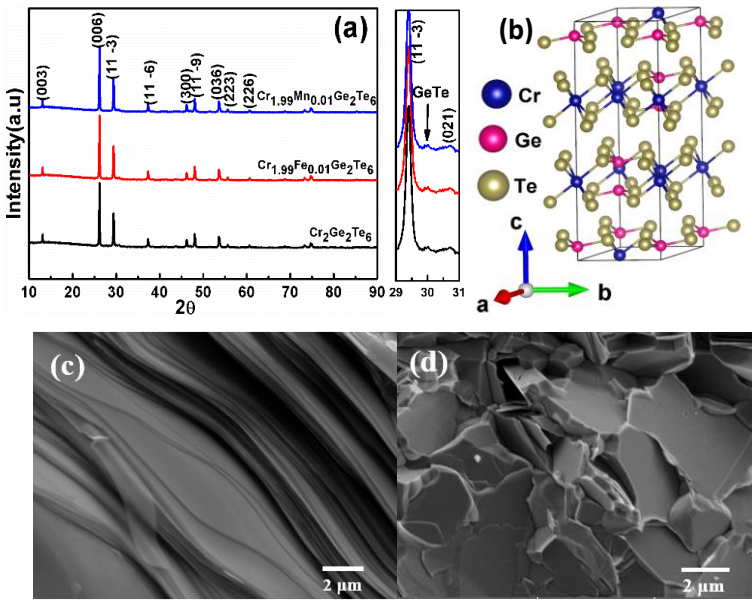

Figure 1. (a) XRD patterns of Mn, Fe doped sample, undoped sample after SPS and enlarged diffraction peaks at 2θ=29° ~31° ; (b) the crystal structure; SEM micrographs of fracture surface, along (c) A direction and (d) P direction of $Cr_2Ge_2Te_6$.

Optimization of Dopants in $Cr_2Ge_2Te_6$ Compounds. As we anticipate that altering the carrier concentration via chemical doping might lead to further promising improvements in the power factor for $Cr_2Ge_2Te_6$. As such, in this study, we practically synthesized Mn-doped and Fe-doped $Cr_2Ge_2Te_6$ samples. Figure 1(a) shows the XRD patterns of $Cr_{1.99}Mn_{0.01}Ge_2Te_6$, $Cr_{1.99}Fe_{0.01}Ge_2Te_6$ and pure $Cr_2Ge_2Te_6$ bulk after SPS. It is clear that the Bragg peaks for all the samples associated with rhombohedral system (space group: R-3) except for a rarely slight GeTe impurity peak at 30°. As shown in Figure 1(b), obviously, the crystal structure of $Cr_2Ge_2Te_6$ is two-dimensional. Tellurium anions closely packed along the c-axis by the weak interlayer van der

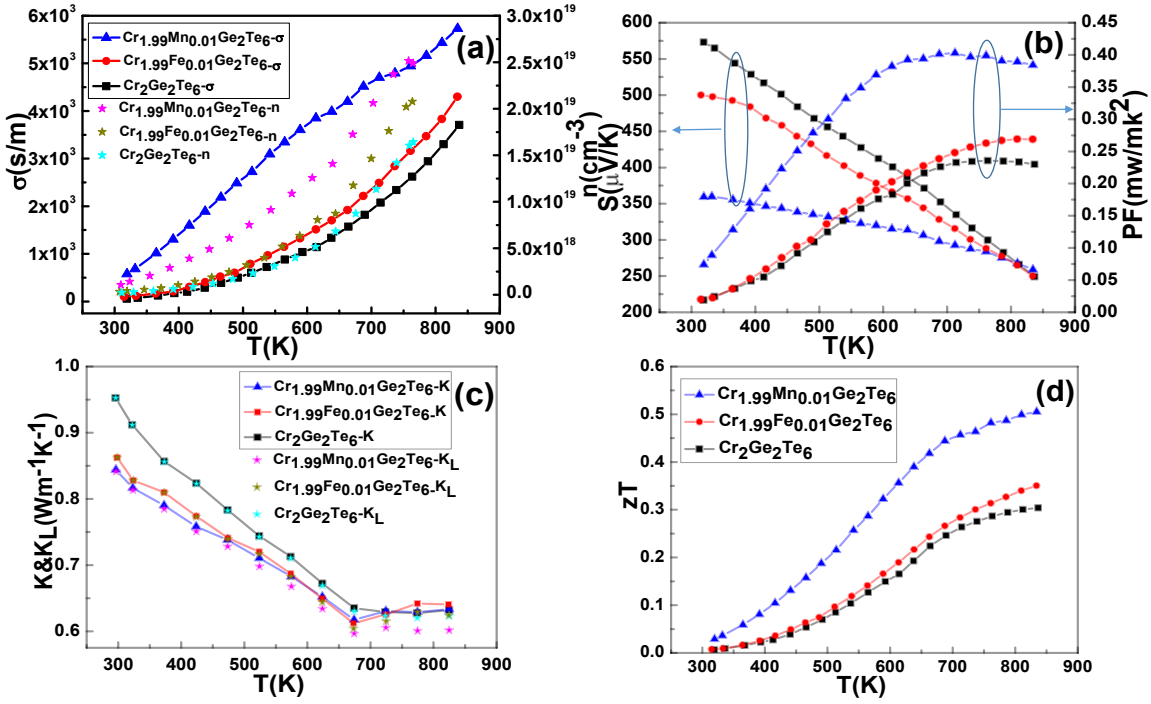

Figure 2. Temperature dependence of (a) electrical conductivity σ and carrier concentration n, (b) Seebeck coefficient and power factor, (c) total thermal conductivity κ and lattice thermal conductivity κ_L, (d) zT for $Cr_2Ge_2Te_6$, $Cr_{1.99}Mn_{0.01}Ge_2Te_6$ and $Cr_{1.99}Fe_{0.01}Ge_2Te_6$ measured along A direction.

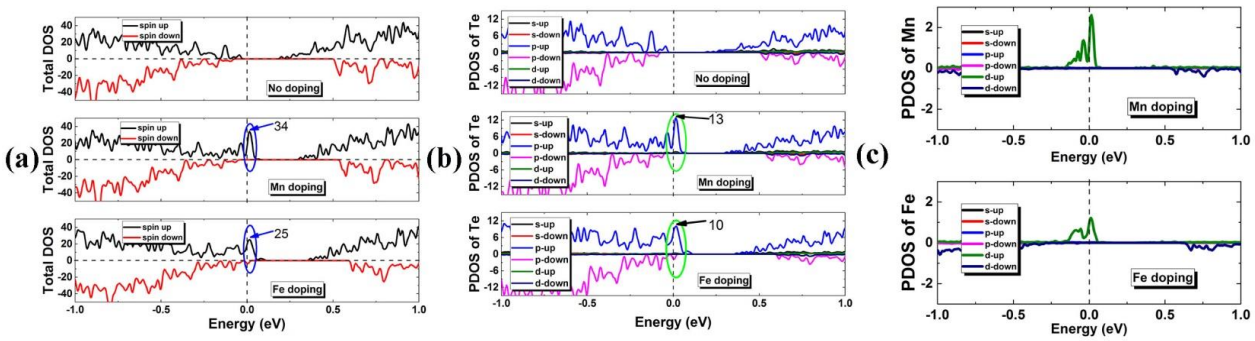

Figure 3. DOS graph of (a) the total DOS of pristine, Mn doped and Fe doped $Cr_2Ge_2Te_6$ (from up to down). The PDOS (Projected density of states) of (b) Te for the pristine, Mn doped and Fe doped $Cr_2Ge_2Te_6$, where it is shown that Te begins to contribute a lot to the DOS around Fermi level upon doping. (c) PDOS of Mn and Fe for the Mn and Fe doped system, respectively.

Waals force, which are easily textured under an applied pressure, showing typical orientation. The two-dimensional nature of the crystal structure is reflected in its morphology. The SEM image of a fully dense SPSed $Cr_{1.9}Mn_{0.1}Ge_2Te_6$ bulk sample along both A and P direction indicates the typical layered texture (see the Figure 1(c)-(d)). The crystal grains are closely packed together and no obvious holes can be found, which corresponds to the high density (more than 95% of theoretical density) of our bulk samples.

The doping effects with different element on thermoelectric properties for $Cr_2Ge_2Te_6$ compounds are investigated for the first time. We synthesize un-doped, Mn-doped, and Fe-doped samples and compare their thermoelectric properties along A direction as present in Figure 2. In Figure 2(a), it is noted that the electrical conductivity σ and carrier concentration n are largely improved via Mn and Fe doping. Furthermore, Mn-doping improves the electric conductivity at a larger degree than that of Fe-doping, which mainly benefits from the higher carriers concentration in Mn doped samples. In Figure 2(b), Seebeck coefficients show a decline trend with temperature while power factors show a reverse trend. The remarkably enhanced electrical conductivity coupled with moderately decreased Seebeck coefficient result in a higher PF via doping and Mn-doped sample possess the highest power factor of 0.40 mW/mK^2. Meanwhile, as shown in Figure 2(c), the total thermal conductivity κ and lattice thermal conductivity κ_L are reduced upon doping due to the introduced impurity scattering.

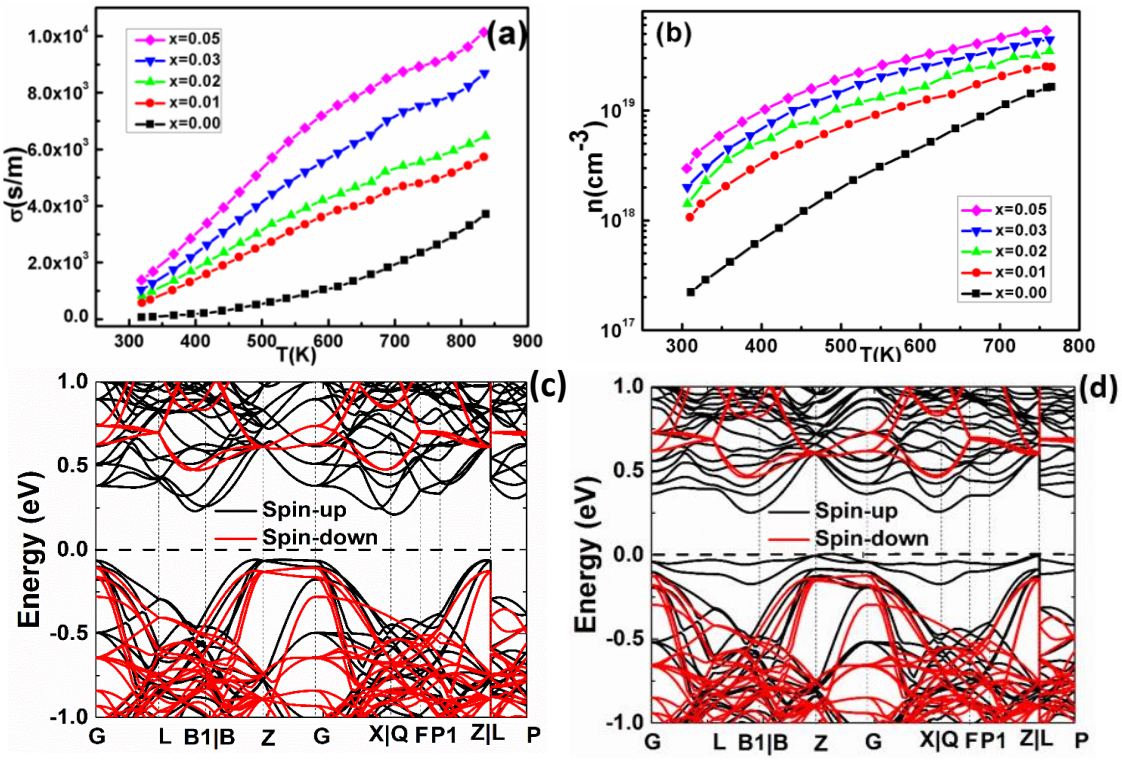

Figure 4. Temperature dependence of (a) electrical conductivity, (b) carrier concentration for $Cr_{2(1-x)}Mn_{2x}Ge_2Te_6$ (x = 0, 0.01, 0.02, 0.03, 0.05) measured along A direction. (c)-(d) band structure of undoped sample and Mn-doped sample.

Mention must be made that slight upturn of κ at ~673 K was observed for all samples, which is attributed to therhombohedral to cubic structural phase transition of GeTe slightly existed in our target samples. Overall, Mn and Fe doping is proved to enhance the thermoelectric properties as shown in Figure 2(d). Besides, Mn-doping is more favorable to improve the electrical properties than Fe doping, which is consistent with our theoretical calculation of DOS as described below.

In order to better understand the doping effect on the transport properties, we calculate the electronic density of states (DOS) of pristine, Mn-doped, and Fe-doped samples. As can be clearly seen from Figure 3(a), there is a significant increase of the DOS around the Fermi level upon doping Mn and Fe into the $Cr_2Ge_2Te_6$ system, especially for the 5*p* orbital of the Te atoms (see Figure 3(b)). As a consequence, the carrier concentration, the electrical conductivity, and thus the *PF* will be enhanced. Compared with Fe doping, we see that Mn doping have relatively larger DOS around the Fermi level, which is consistent with the fact that Mn doping is more favorable to improve the electrical properties as discussed above. By a detailed analysis of the projected DOS on each atom, it is further found that the DOS of *p* orbital from Te atoms around Fermi level has a similar shape with that of the *d* orbital of doped atoms M (M = Fe, Mn) (shown in Figure 3(c)), which indicates an orbital hybridization between them, and is considered to be the origin of the impurity energy level as discussed below in the band structure. Note that the asymmetric DOS near Fermi level between spin-up and down for the intrinsic nonmagnetic atoms (See Figure 3(b) and Figure S1) indicates a spin polarization, which is caused by the strong magnetic atoms Cr. This can be confirmed by that the calculated magnetic moment of Cr, Ge, Te atoms, which are 3.102, 0.024, −0.140 μ_b per atom, respectively.

Optimization of the Amount of Mn Doping in $Cr_2Ge_2Te_6$ Compounds. Figure 4(a)-(b) show the temperature dependent electrical conductivity and carrier concentration of $Cr_{2(1-x)}Mn_{2x}Ge_2Te_6$ (x = 0, 0.01, 0.02, 0.03, 0.05) measured along A direction. Obviously, in Figure 4(a), all the electrical conductivities increase with temperature, which is a typical semiconductor behavior. For Mn-doped samples, the peak electrical conductivities is highly enhanced from 3700 s/m to 10957 s/m along A direction, due to the monotonically increasing carrier concentration which is shown in Figure 4(b). Besides, electrical conductivity values along P direction (showed in Figure S5(a)) are larger than those along A pressing direction, which is consistent with our previous study.[23] It is interesting to note that Mn substitution on Cr site increases the hole concentration although Mn is supposed to donate electrons. To address this problem, we calculated the spin polarized band structure of pristine and Mn-doped $Cr_2Ge_2Te_6$ systems, as shown in Figure 4(c)-(d). In principle, the replacement of Cr site with Mn atom would introduce additional electrons, leading to an upshift of the Fermi level. This deduction correspond to the fact that the Fermi level is away from the valence band maximum (VBM) with the energy difference increase from 0.06 eV to 0.08 eV (in the absence of the two introduced bands in the doped system) according to our theoretical results. Thus an decrease of hole concentration is expected. However, the doping of Mn introduces two impurity bands above the VBM of the undoped system and the Fermi level almost crosses to the new VBM, which indicates a large DOS near Fermi level and thus could highly increase the holes concentration. It is worthwhile to

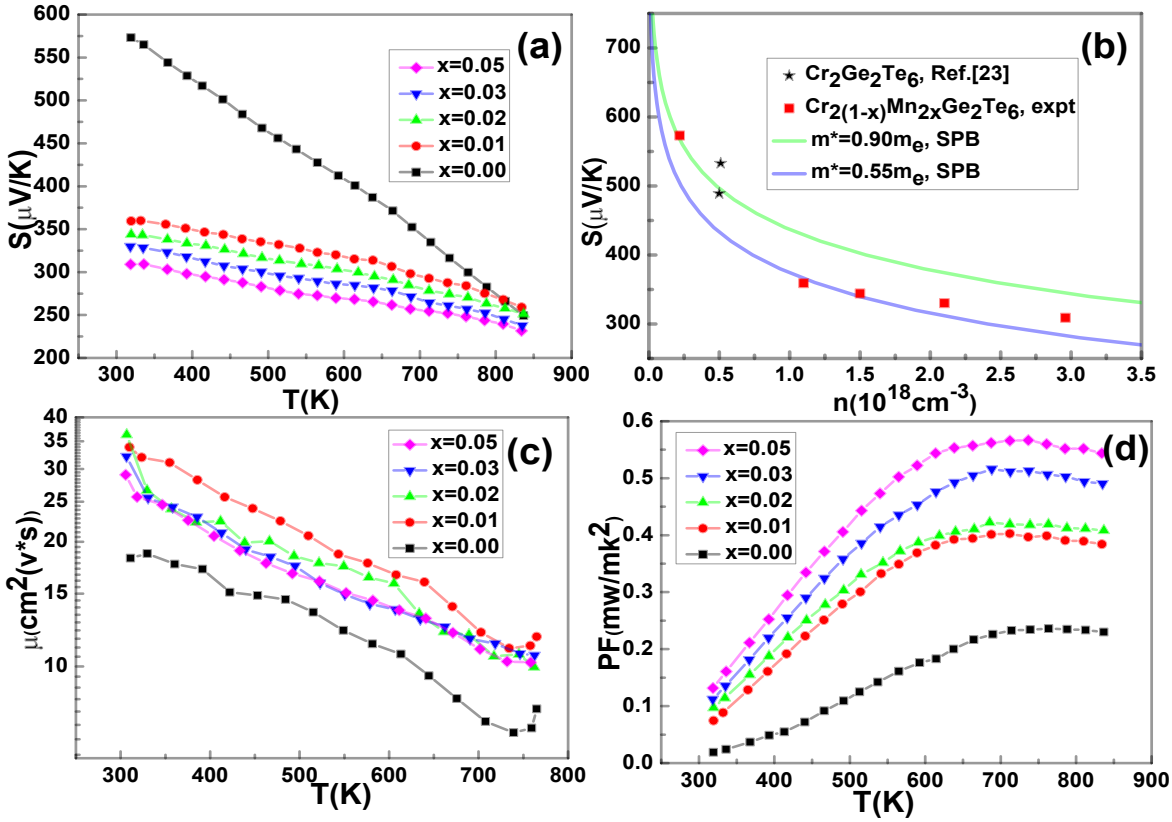

Figure 5. Temperature dependence of (a) Seebeck coefficient and (b) room temperature Pisarenko relation; The green curve represent the predicted results from the single parabolic band model with an effective mass of 0.90m_e for un-doped sample and blue curve for Mn-doping samples with 0.55m_e. (c) carrier mobility; (d) power factor for $Cr_{2(1-x)}Mn_{2x}Ge_2Te_6$ (x = 0, 0.01, 0.02, 0.03, 0.05) along A direction.

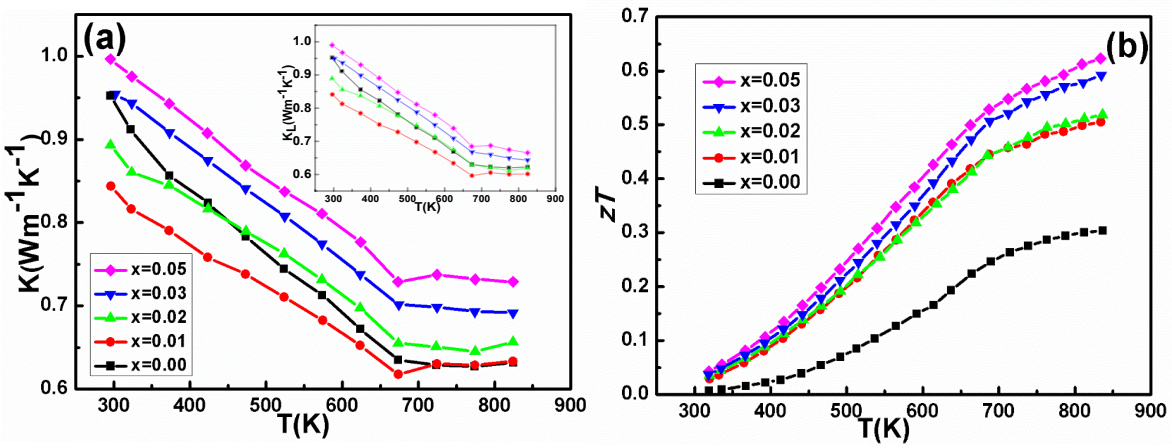

Figure 6. (a)Total thermal conductivity and lattice thermal conductivity showed in the inset; (b) *zT* for $Cr_{2(1-x)}Mn_{2x}Ge_2Te_6$ (x = 0, 0.01, 0.02, 0.03, 0.05) measured along A direction.

mention that the dispersion of the top impurity band along Z-G direction (Figure 4(d)) is greater than the bands near VBM for un-doped system (Figure 4(c)), suggesting the smaller effective mass in Mn-doped samples.

The positive Seebeck coefficient values shown in Figure 5(a) indicate that the prepared samples are p-type and majority of charge carriers are holes. The Seebeck coefficient decreases with increasing Mn-doping content at the same temperature but still remain robust, and the values along A direction at room temperature are 570, 359, 344, 330, 309 μV/K for x = 0, 0.01, 0.02, 0.03, 0.05, respectively. Such reduced Seebeck coefficient is due to the increase of carrier concentration upon Mn doping. Furthermore, based on the room temperature Pisarenko line as shown in Figure 5(b) by employing a single parabolic band (SPB) model under the relaxation time approximation and the electrical transport dominated by acoustic phonon scattering, it is found that the effective mass of the pure sample is around 0.90 m_e, which is consistent with the previous report [23]. However, the effective mass of Mn doped samples are all around 0.55 m_e. Such trend is in good agreement with our theoretical calculation as mentioned above. The exact values of effective mass for each samples are shown in Figure S6. Figure 5(c) shows the temperature dependence of the carrier mobility. It is noted that the values of doped samples is higher than that of the pure $Cr_2Ge_2Te_6$. This enhancement of carrier mobility can be explained by the decrease of effective mass in doped samples. The enhanced electrical conductivity combined with the decent Seebeck coefficient contribute to a moderate power factor of 0.57 mW/mK^2 for $Cr_{1.9}Mn_{0.1}Ge_2Te_6$ at 760 K along A direction (shown in Figure 5(d)). It is clear that the electrical property have been highly improved by optimizing the carrier concentration through successful Mn doping of $Cr_2Ge_2Te_6$.

The total thermal conductivity κ and lattice thermal conductivity κ_L of $Cr_{2(1-x)}Mn_{2x}Ge_2Te_6$ (x = 0, 0.01, 0.02, 0.03, 0.05) measured along A direction are showed in Figure 6(a). For all samples, the total thermal conductivities κ in both two direction decrease with temperature below 680 K due to Umklapp scattering. Furthermore, the κ along A direction are much lower than that along P direction (see Figure S5(d)), which may be explained by the typical layered structure since phonons can be scattered by the interfaces between each layer and the weak bonding between layers.[35,36] The electronic thermal conductivity is calculated by the formula $\kappa_e = L\sigma T$, where L is the Lorenz number. Here a constant Lorenz number of 1.5×10^{-8} V^{2}K^{-2} is used.[23] The estimation of the lattice thermal conductivity κ_L is obtained by subtracting the electronic component κ_e from the total thermal conductivity, $\kappa_L = \kappa - \kappa_e$. Considering the relatively low electronic thermal conductivity κ_e, the lattice thermal conductivity κ_L (the inset in Figure 6(a)) is nearly similar to the total thermal conductivity, showing the same behavior as other reported materials such as SnSe,[5,21,37] BiCuSeO.[38] In Figure 6(b), *zT* values increase with the increasing temperature as well as the increasing doping content of Mn. The peak *zT* value for doped sample is about 0.63 along A direction at 830 K with x = 0.05, which is almost twice as much as that of un-doped sample in the same direction and the same temperature. Such enhancements in *zT* mostly benefit from the improved power factor and the low intrinsic thermal conductivity. In this work, Mn doping increase the carrier concentration due to the presence of two impurity bands above the valence band maximum (VBM), leading to the significant increase of the electrical conductivity. However, the Fermi level has not been shifted inside the valence band upon doping. As a consequence, a much larger *zT* value can be anticipated assuming the Fermi level can be shifted successfully.

■ CONCLUSIONS

In summary, p-type $Cr_{2(1-x)}Mn_{2x}Ge_2Te_2$ (x = 0, 0.01, 0.02, 0.03, 0.05) and $Cr_{1.99}Fe_{0.01}Ge_2Te_6$ compounds were synthesized by solid-state reaction followed by spark plasma sintering. It is found that Mn and Fe doping introduces the two impurity bands yielded by the orbital hybridization between *d* orbitals of the doping atom and the *p* orbital of Te. These two impurity bands increase the carrier concentration, leading to the enhancement of the electrical properties and Mn doping is more effective. Combined with the intrinsic thermal conductivity, a peak *zT* ~0.63 at 833 K along A direction in $Cr_{1.9}Mn_{0.1}Ge_2Te_6$ is obtained, a twofold value as compared to the un-doped sample at the same direction and temperature. Further improvement of the thermoelectric performance can be obtained by shifting the Fermi level in the doped $Cr_2Ge_2Te_6$ compounds.

■ ASSOCIATED CONTENT

Supporting Information

The projected DOS of the pristine, Mn-doped and Fe-doped $Cr_2Ge_2Te_6$; SEM micrographs of fracture surface for $Cr_{1.9}Mn_{0.1}Ge_2Te_6$ along A and P direction; TEM and HRTEM images of $Cr_{1.9}Mn_{0.1}Ge_2Te_6$; XRD patterns of $Cr_{2(1-x)}Mn_{2x}Ge_2Te_6$ (x = 0, 0.01, 0.02, 0.03, 0.05) and enlarged diffraction peaks at $2\theta=29^o$ ~31^o ; Temperature dependence of electrical conductivity, Seebeck coefficient, power factor, total thermal conductivity, lattice thermal conductivity, and *zT* for $Cr_{2(1-x)}Mn_{2x}Ge_2Te_6$ (x = 0,

0.01, 0.02, 0.03, 0.05) measured along P direction; Effective mass for $Cr_{2(1-x)}Mn_{2x}Ge_2Te_6$ (x = 0, 0.01, 0.02, 0.03, 0.05) along A direction.

The Supporting Information is available free of charge on the ACS Publications website at DOI: …..

AUTHOR INFORMATION

Corresponding Author

* Professor Xiaoyuan Zhou: xiaoyuan2013@cqu.edu.cn

* Professor Huijun Liu: phlhj@whu.edu.cn

Notes

The authors declare no competing financial interests.

ACKNOWLEDGMENT

This work was financially supported in part by the National Natural Science Foundation of China (Grant Nos. 11344010, 11404044, 51472036), the Fundamental Research Funds for the Central Universities (106112016CDJZR308808). The work conducted at the Chongqing Institute of Green and Intelligent Technology, Chinese Academy of Sciences is supported by the 100 Talent Program of the Chinese Academy of Sciences (Grant No. 2013-46), the National Natural Science Foundation of China (Grant Nos.51672270, 51401202), and the Project for Fundamental and Frontier Research in Chongqing (CSTC2015JCYJBX0026). We would also acknowledge the support from Prof. Yanzhong Pei at Tongji University for the high temperature hall measurement.

REFERENCES

(1) DiSalvo, F. Thermoelectric Cooling and Power Generation. *Science* (80-.). 1999, 285 (5428), 703–706.

(2) Yang, J.; Caillat, T. Thermoelectric Materials for Space and Automotive Power Generation. *MRS Bulletin*, 31(3), 224-229.

(3) Snyder, G. J.; Toberer, E. S. Complex Thermoelectric Materials. *Nature materials.* 2008, 7 (2), 105–114.

(4) Zhou, X.; Wang, G.; Guo, L.; Chi, H.; Wang, G.; Zhang, Q.; Chen, C.; Thompson, T.; Sakamoto, J.; Dravid, V.; Cao, G.; Uher, C. Hierarchically Structured TiO2 for Ba-Filled Skutterudite with Enhanced Thermoelectric Performance. *J. Mater. Chem. A* 2014, 20629–20635.

(5) Zhang, Q.; Chere, E. K.; Sun, J.; Cao, F.; Dahal, K.; Chen, S.; Chen, G.; Ren, Z. Studies on Thermoelectric Properties of N-Type Polycrystalline $SnSe_{1-x}S_x$ by Iodine Doping. *Adv. Energy Mater.* 2015, 5 (12), 1–8.

(6) Pei, Y.; Heinz, N. a.; LaLonde, A.; Snyder, G. J. Combination of Large Nanostructures and Complex Band Structure for High Performance Thermoelectric Lead Telluride. *Energy Environ. Sci.* 2011, 4 (9), 3640-3645.

(7) Zhang, Q.; Cao, F.; Liu, W.; Lukas, K.; Yu, B.; Chen, S.; Opeil, C.; Broido, D.; Chen, G.; Ren, Z. Heavy Doping and Band Engineering by Potassium to Improve the Thermoelectric Figure of Merit in P-Type PbTe, PbSe, and $PbTe_{1-y}Se_y$. *J. Am. Chem. Soc.* 2012, 134 (24), 10031–10038.

(8) Pei, Y.; Shi, X.; Lalonde, A.; Wang, H.; Chen, L.; Snyder, G. J. Convergence of Electronic Bands for High Performance Bulk Thermoelectrics. *Nature* 2011, 473 (7345), 66–69.

(9) Li, W.; Chen, Z.; Lin, S.; Chang, Y.; Ge, B.; Chen, Y.; Pei, Y. Band and Scattering Tuning for High Performance Thermoelectric $Sn_{1-x}Mn_xTe$ Alloys. *J. Mater.* 2015, 1 (4), 1–9.

(10) Martin, J.; Wang, L.; Chen, L.; Nolas, G. S. Enhanced Seebeck Coefficient through Energy-Barrier Scattering in PbTe Nanocomposites. *Phys. Rev. B - Condens. Matter Mater. Phys.* 2009, 79 (11), 1–5.

(11) Bahk, J. H.; Bian, Z.; Shakouri, A. Electron Energy Filtering by a Nonplanar Potential to Enhance the Thermoelectric Power Factor in Bulk Materials. *Phys. Rev. B - Condens. Matter Mater. Phys.* 2013, 87 (7), 075204.

(12) Harman, T. C.; Taylor, P. J.; Walsh, M. P.; La Forge, B. E. Quantum Dot Superlattice Thermoelectric Materials and Devices. *Science* (80-.). 2002, 297, 2229–2232.

(13) Heremans, J. P.; Wiendlocha, B.; Chamoire, A. M. Resonant Levels in Bulk Thermoelectric Semiconductors. *Energy Environ. Sci.* 2012, 5 (2), 5510–5530.

(14) Morelli, D. T.; Meisner, G. P. Low Temperature Properties of the Filled Skutterudite $CeFe_4Sb_{12}$. *J. Appl. Phys.* 1995, 77 (8), 3777-3781.

(15) Keppens, V.; Mandrus, D.; Sales, B. C.; Chakoumakos, B. C.; Dai, P.; Coldea, R.; Maple, M. B.; Gajewski, D. a; Freeman, E. J.; Bennington, S. Localized Vibrational Modes in Metallic Solids. *Lett. to Nat.* 1998, 395 (10), 876–878.

(16) Li, Z.; Xiao, C.; Fan, S.; Deng, Y.; Zhang, W.; Ye, B.; Xie, Y. Dual Vacancies: An Effective Strategy Realizing Synergistic Optimization of Thermoelectric Property in BiCuSeO. *J. Am. Chem. Soc.* 2015, 137 (20), 6587–6593.

(17) Jiang, G.; He, J.; Zhu, T.; Fu, C.; Liu, X.; Hu, L.; Zhao, X. High Performance $Mg_2(Si,Sn)$ Solid Solutions : A Point Defect Chemistry Approach to Enhancing Thermoelectric Properties. *Adv. Funct. Mater.* 2014, 24, 3776–3781

(18) Zhao, L. D.; Wu, H. J.; Hao, S. Q.; Wu, C. I.; Zhou, X. Y.; Biswas, K.; He, J. Q.; Hogan, T. P.; Uher, C.; Wolverton, C.; Dravid, V. P.; Kanatzidis, M. G. All-Scale Hierarchical Thermoelectrics: MgTe in PbTe Facilitates Valence Band Convergence and Suppresses Bipolar Thermal Transport for High Performance. *Energy Environ. Sci.* 2013, 6 (11), 3346–3355.

(19) Li, W.; Lin, S.; Ge, B.; Yang, J.; Zhang, W.; Pei, Y. Low Sound Velocity Contributing to the High Thermoelectric Performance of Ag_8SnSe_6. *Adv. Sci.* 2016, 3(11), 1600196.

(20) Shi, X.; Kong, H.; Li, C.-P.; Uher, C.; Yang, J.; Salvador, J. R.; Wang, H.; Chen, L.; Zhang, W. Low Thermal Conductivity and High Thermoelectric Figure of Merit in N-Type $Ba_xYb_yCo_4Sb_{12}$ Double-Filled Skutterudites. *Appl. Phys. Lett.* 2008, 92 (18), 182101.

(21) Zhao, L.-D.; Lo, S.-H.; Zhang, Y.; Sun, H.; Tan, G.; Uher, C.; Wolverton, C.; Dravid, V. P.; Kanatzidis, M. G. Ultralow Thermal Conductivity and High Thermoelectric Figure of Merit in SnSe Crystals. *Nature* 2014, 508 (7496), 373–377.

(22) Biswas, K.; He, J.; Blum, I. D.; Wu, C.-I.; Hogan, T. P.; Seidman, D. N.; Dravid, V. P.; Kanatzidis, M. G. High-Performance Bulk Thermoelectrics with All-Scale Hierarchical Architectures. *Nature* 2012, 489 (7416), 414–418.

(23) Yang, D.; Yao, W.; Chen, Q.; Peng, K.; Jiang, P.; Lu, X.; Uher, C.; Yang, T.; Wang, G.; Zhou, X. $Cr_2Ge_2Te_6$: High Thermoelectric Performance from Layered Structure with High Symmetry. *Chem. Mater.* 2016, 28 (6), 1611–1615.

(24) Wu, L.; Yang, J.; Chi, M.; Wang, S.; Wei, P.; Zhang, W. Enhanced Thermoelectric Performance in Cu-Intercalated BiTeI by Compensation Weakening Induced Mobility Improvement. *Sci Rep.* 2015, 5: 14319.

(25) Qiu, W.; Xi, L.; Wei, P.; Ke, X.; Yang, J.; Zhang, W. Part-Crystalline Part-Liquid State and Rattling-like Thermal Damping in Materials with Chemical-Bond Hierarchy. *Proc. Natl. Acad. Sci. U. S. A.* 2014, 111 (42), 15031–15035.

(26) Qiu, W.; Wu, L.; Ke, X.; Yang, J.; Zhang, W. Diverse Lattice Dynamics in Ternary Cu-Sb-Se Compounds. *Sci. Rep.* 2015, 5, 13643.

(27) Zhang, Y.; Ke, X.; Kent, P. R. C.; Yang, J.; Chen, C. Anomalous Lattice Dynamics near the Ferroelectric Instability in PbTe. *Phys. Rev. Lett.* 2011, 107 (17), 175503.

(28) Ji, H.; Stokes, R. A.; Alegria, L. D.; Blomberg, E. C.; Tanatar, M. A.; Reijnders, A.; Schoop, L. M.; Liang, T.; Prozorov, R.; Burch, K. S.; Ong, N. P.; Petta, J. R.; Cava, R. J. A Ferromagnetic Insulating Substrate for the Epitaxial Growth of Topological Insulators. *J. Appl. Phys.* 2013, 114 (11), 1–7.

(29) Kresse, G.; Hafner, J. Ab Initio Molecular Dynamics for Open-Shell Transition Metals. *Phys. Rev. B* 1993, 48 (17), 13115–13118.

(30) Kresse, G.; Hafner, J. Ab Initio Molecular-Dynamics Simulation of the Liquid-Metal–amorphous-Semiconductor Transition in Germanium. *Phys. Rev. B* 1994, 49 (20), 14251–14269.

(31) Kresse, G.; Furthmüller, J. Efficient Iterative Schemes for Ab Initio Total-Energy Calculations Using a Plane-Wave Basis Set. *Phys. Rev. B* 1996, 54 (16), 11169–11186.

(32) Perdew, J. P.; Burke, K.; Ernzerhof, M. Generalized Gradient Approximation Made Simple. Phys. Rev. Lett. 1996, 77 (18), 3865–3868.

(33) Anisimov, V. I.; Zaanen, J.; Andersen, O. K. Band Theory and Mott Insulators: Hubbard U instead of Stoner I. *Phys. Rev. B* 1991, 44 (3), 943–954.

(34) Curtarolo, S.; Setyawan, W.; Hart, G. L. W.; Jahnatek, M.; Chepulskii, R. V.; Taylor, R. H.; Wang, S.; Xue, J.; Yang, K.; Levy, O.; Mehl, M. J.; Stokes, H. T.; Demchenko, D. O.; Morgan, D. AFLOW: An Automatic Framework for High-Throughput Materials Discovery. *Comput. Mater. Sci.* 2012, 58, 218–226.

(35) Venkatasubramanian, R.; Siivola, E.; Colpitts, T.; O'Quinn, B. Thin-Film Thermoelectric Devices with High Room-Temperature Figures of Merit. *Nature* 2001, 413 (6856), 597–602.
(36) Zhao, X. B.; Ji, X. H.; Zhang, Y. H.; Zhu, T. J.; Tu, J. P.; Zhang, X. B. Bismuth Telluride Nanotubes and the Effects on the Thermoelectric Properties of Nanotube-Containing Nanocomposites. *Appl. Phys. Lett.* 2005, 86 (6), 1–3.
(37) Chen, C.-L.; Wang, H.; Chen, Y.-Y.; Day, T.; Snyder, J. Thermoelectric Properties of P-Type Polycrystalline SnSe Doped with Ag. *J. Mater. Chem. A* 2014, 2 (29), 11171–11176.
(38) Li, J.; Sui, J.; Pei, Y.; Barreteau, C.; Berardan, D.; Dragoe, N.; Cai, W.; He, J.; Zhao, L.-D. A High Thermoelectric Figure of Merit ZT > 1 in Ba Heavily Doped BiCuSeO Oxyselenides. *Energy Environ. Sci.* 2012, 5 (9), 8543-8547.

Table of Contents Graphic